Chapter 4

INTEGRATION OF ELECTROCATALYSTS WITH SILICON MICROCONE ARRAYS FOR MINIMIZATION OF OPTICAL AND OVERPOTENTIAL LOSSES DURING SUNLIGHT-DRIVEN HYDROGEN EVOLUTION

Yalamanchili, S.,* Kempler, P. A.,* Papadantonakis, K. M., Atwater, H. A., & Lewis, N. S. (2019). Integration of electrocatalysts with silicon microcone arrays for minimization of optical and overpotential losses during sunlight-driven hydrogen evolution. *Sustainable Energy & Fuels*, 3(9), 2227-2236. https://doi.org/10.1039/C9SE00294D

4.1 Introduction

Polished Si photocathodes exhibit light-limited photocurrent densities $|J_{ph}| < 29$ mA cm^{-2}, due to optical losses arising from front-surface reflection.[97] $|J_{ph}|$ can approach the theoretical maximum of ~ 44 mA cm^{-2} for Si under 100 mW cm^{-2} of Air Mass 1.5 illumination[98] by use of an antireflective coating, combined with surface texturing such as micropyramids (μ–pyramids) produced by anisotropic wet-chemical etching, or by high-aspect ratio structuring of the Si.[43, 99-101] Antireflective coatings such as SiO_2, Si_3N_4, or Al_2O_3, as commonly used in photovoltaic devices, are not catalytically active or electronically conductive; the use of such materials in a photoelectrode system in which charge-transfer occurs across the illuminated solid/liquid interface requires separation of regions responsible for charge transfer and light absorption.[93, 102] Si photocathodes with a

passivated front surface and Pt loaded on the rear surface, out of the path of incident light, exhibit photovoltages in excess of 630 mV under 1 Sun illumination and exhibit limiting photocurrent densities that are relatively independent of the mass loading of electrocatalyst.[103]

Most of the highly active catalysts for fuel production reflect and parasitically absorb light in the solar spectrum. These optical losses by the catalyst can be reduced by decreasing the catalyst loading to increase transmissivity;[104] by developing transparent and antireflective catalysts;[51, 105] by depositing the catalyst as islands rather than as a continuous film;[106] and/or by strategically placing the catalyst out of the path of incident light on three-dimensionally structured Si substrates.[40] On planar surfaces, increases in the catalyst loading and/or surface coverage decrease the effective current density at the catalyst, so the reduced overpotential and consequent increase in fill factor can partially offset the efficiency losses that would otherwise result from a decrease in $J_{ph.}$[106] The ideal electrode microstructure would therefore simultaneously minimize reflection and absorption losses in the catalyst while optimizing the catalyst loading to reduce the overpotential required to convert photogenerated charge carriers into fuel.

H_2-evolving Si photocathodes have been made using surface texturing such as μ-pyramids, [51, 107] nanowires,[50, 108-110] and microwires (μ-wires).[30, 39, 54, 104] Light-limited current densities as high as $|J_{ph}| = 43$ mA cm^{-2} have been reported for Si μ-pyramids coated with a highly transparent and potentially antireflective MoS_xCl_y catalyst grown by chemical-vapor deposition.[51] A photocurrent density at the reversible hydrogen electrode (RHE) potential, $J_{RHE} = -37.5$ mA cm^{-2} was obtained for over 30 min, using a transparent $NiCoSe_x$ catalyst formed via light-assisted electrodeposition onto Si nanowire array

photocathodes.[50] For Si microwires (μ-wires), J_{RHE} = -35.5 mA cm^{-2} was obtained by optimizing both the coverage of an electrodeposited Ni-Mo catalyst on the μ-wires and the pitch of the μ–wires.[54] Replacing the catalyst in these structures with thin Pt (~ 5 nm or less), which is widely used because of its high activity and stability in corrosive environments, led to substantial optical absorption and reflection losses, and produced a decrease of 5–7 mA cm^{-2} in $|J_{RHE}|$.[50-51, 54]

Polymer-embedded Si μ-wires with an antireflective Si_3N_4 coating and scattering particles can absorb up to 84.4% of the incident radiation at normal incidence, which is above the light-trapping limit for an equivalently thick Si substrate.[30, 111] However, widely spaced Si μ-wires on a Si substrate reflect >30% of normally incident light, due to the flat tops of the μ–wires. In contrast, tapering the cylindrical shape of Si μ-wires into Si microcones (μ-cones) with a tip curvature of 25 nm enhances the absorption of Si to > 90% at normal incidence, equivalent to 99.5% of the classical broadband light-trapping limit, with above-the-limit absorption observed at long wavelengths.[43, 101] Such Si μ-cones reflect only ~1% of normally incident light, which is comparable to the reflection from black silicon substrates.[99-100, 112] This behavior arises from the coupling of broad-band light to multiple available waveguide modes whose resonance exists at various radii resulting from the conical geometry.[43, 113-114] The high surface area for catalyst loading provided by the μ–cone geometry makes Si μ-cones an attractive architecture for Si photocathodes in hydrogen-producing systems. Herein we investigate the H_2-evolution performance of Si μ-cone array photocathodes coupled with either a highly active but reflective thin film of Pt catalyst, or with a discontinuous film of Co-P as an example of an electrocatalyst composed of earth-abundant elements. Si μ-cones were removed from the substrate in a

flexible polymer support leading to devices which demonstrated H_2 evolution at potentials positive of RHE.

4.2 Experimental Methods

(Photo)electrochemical measurements: The performance of photocathodes for photoelectrochemical hydrogen evolution was measured in H_2-purged 0.50 M H_2SO_4(aq) (TraceMetals grade, Fisher) under 100 mW cm^{-2} of simulated AM1.5 illumination produced by a filtered Hg (Xe) lamp powered at 290 W. A Biologic SP-200 was used for the potentiostat, and the electrochemical cell had a three-electrode configuration. A Ag/AgCl (Saturated KCl) or Saturated Calomel reference electrode was calibrated against the RHE potential using a platinum-black electrode, and a graphite rod positioned behind a porous glass frit served as the counter electrode. Current density vs potential, *J-E*, data were obtained by sweeping the potential at 50 mV s^{-1} from open circuit to -0.2 V vs RHE. The electrolyte was stirred rapidly with a magnetic stir bar, to remove hydrogen bubbles from the surface of the device.

Spectral response measurements: The external quantum yield of n^+p-Si/Ti/Pt and p-Si/Co-P μ–cone arrays were recorded using a Biologic VMP3 Multichannel potentiostat connected to a lock-in amplifier with illumination from a Xe lamp powered at 150 W passed through a monochromator controlled via LabView and chopped at 10-15 Hz. Spectra were referenced to a calibrated reference diode (Thorlabs FDS100-CAL). The potential of p-Si/Co-P photocathodes was held at -200 mV vs RHE to ensure that the sample remained under reductive bias in the dark, while the potential of n^+p-Si/Ti/Pt photocathodes was held at 0 V vs RHE.

Details on the fabrication of n^+p-Si/Pt, p-Si/Co-P μ–cones, and membrane embedded photocathodes, as well as experimental procedures for stability testing are provided in the Appendix (**A.4**).

4.3 Results and Discussion

4.3.1 Homojunction Si photocathodes with sputtered Pt catalyst

Arrays of Si μ-cones with n^+p homojunctions were prepared by inductively coupled plasma reactive-ion etching (ICP-RIE) of a patterned <100>-oriented p-type Si wafer, followed by diffusion doping with P to form the n^+ emitter layer (experimental details are provided in the Appendix (**A.1 and A.4**) **Figure 4.1** (**A-F**) schematically shows the fabrication process for the n^+p-Si μ-cone array photocathodes, with the tips of the μ-cones supporting a Pt catalyst (n^+p-Si/Pt μ–cones) for the hydrogen-evolution reaction (HER). **Figure 4.1G** shows a scanning-electron micrograph (SEM) of a cross section of an as-prepared n^+p-Si/Pt μ–cone array photocathode with Pt covering 6-9 μm at the tips of the μ-cones.

Figure 4.2 compares the current density vs potential (*J-E)* behavior under 100 mW cm^{-2} of simulated AM1.5 illumination for varied thicknesses of Pt deposited onto as-fabricated n^+p-Si/Pt μ-cone array photocathodes, planar n^+p-Si/Pt photocathodes, and pyramidally-textured n^+p-Si/Pt photocathodes (μ–pyramid), when operated in contact with H_2-saturated 0.50 M H_2SO_4(aq). Of the three photocathode geometries, the μ–cone array exhibited the highest light-limited photocurrent density $|J_{ph}|$ (at large negative biases, < -1.5 V versus RHE).

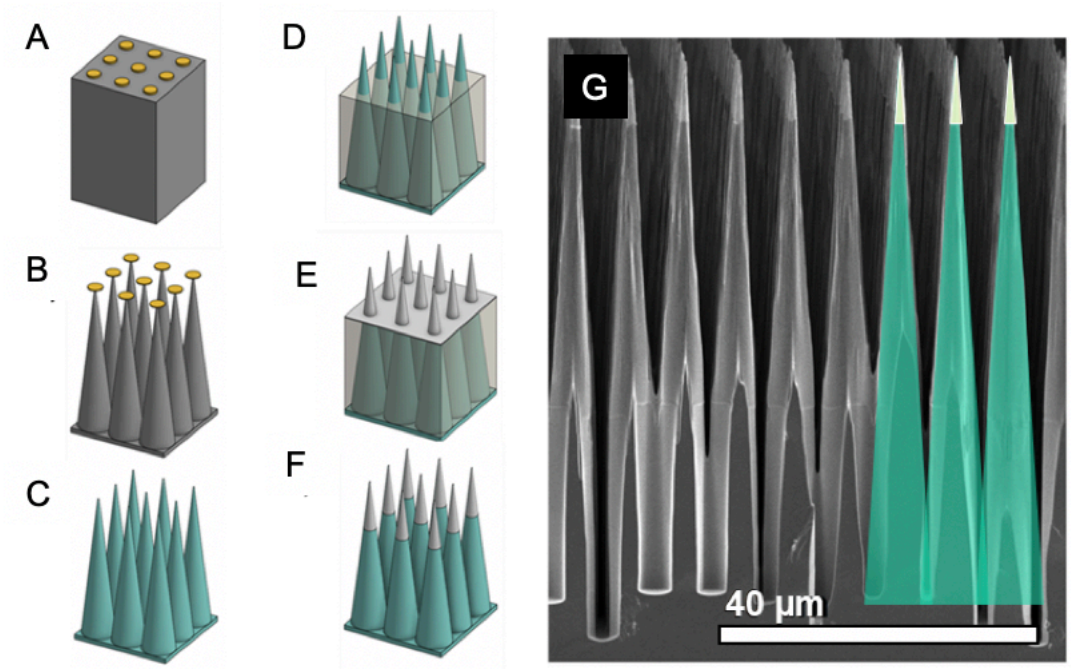

Figure 4.1: (**A-F**) Schematic for the fabrication of n^+p-Si µ–cone array photocathodes with Pt selectively loaded on the tips of the µ-cones. (**A**) Aluminum oxide mask (yellow) patterned on p-type silicon (gray). (**B**) Controlled undercutting of the etch mask leads to high-aspect ratio cones. (**C**) Removal of the etch mask followed by formation of an n^+-emitter layer (green) via phosphorus doping. (**D**) Infilling with wax (transparent gray) followed by directional O_2 etching to expose tips. (**E**) Uniform deposition of Pt via sputtering. (**F**) Removal of the wax with acetone leaves Pt only at the cone tips. (**G**) Scanning-electron micrograph of n^+p-Si µ–cone photocathodes with Pt selectively deposited on the tips of the µ-cones

The overpotential required for the HER decreased as Pt was added to the photocathodes. For the planar and µ–pyramid geometries, increasing the thickness of the Pt resulted in improvements to the fill factors (*ff*) of the *J-E* characteristic; however, increasing the thickness of the Pt catalyst beyond 2 nm resulted in reductions to $|J_{ph}|$ due to optical absorption and reflection losses associated with the Pt layer. For the planar and µ–pyramid geometries, $-J_{RHE}$ decreased to < 10 mA cm^{-2} when the thickness of the Pt layer

reached 8 nm or 16 nm, respectively. However, Si μ-cone array photocathodes with 8 nm of Pt yielded - J_{RHE} = 33 ± 2 mA cm^{-2}, only ~6% less than -J_{ph} = 35.0 mA cm^{-2} observed for bare n$^+$p-Si μ–cone photocathode arrays (**Figure 4.2D**). For n$^+$p-Si/Pt μ–cone array photocathodes with 8 nm of Pt, the voltage required to drive the HER at a rate corresponding to a current density of -10 mA cm^{-2}, V_{-10}, was -70 mV relative to the open-circuit potential (E_{oc}). Doubling the thickness of the Pt layer, from 8 nm to 16 nm, on the tips of the μ–cones resulted in a slight decrease in - J_{RHE}, to 31 ± 3 mA cm^{-2}, but did not change V_{-10}. The addition of a titanium adhesion layer between the Si and Pt did not change V_{oc} or V_{-10} and did not produce a decrease in $|J_{ph}|$ relative to the bare n$^+$p-Si μ–cone array.

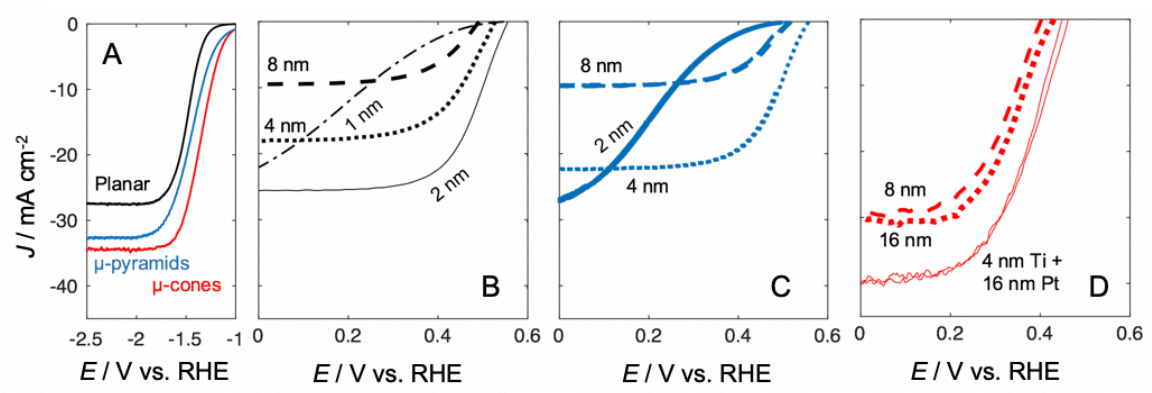

Figure 4.2: Effect of Pt loading on the *J-E* behavior of n$^+$p-Si photocathodes with planar (black traces), μ-pyramid (blue traces), and μ-cone array (red traces) morphologies, as measured in contact with H_2-saturated 0.50 M H_2SO_4(aq) while illuminated by 100 mW cm^{-2} of simulated Air Mass (AM) 1.5 illumination. (**A**) *J-E* behavior of bare (no Pt) n$^+$p-Si photocathodes. Representative *J-E* behavior for n$^+$p-Si/Pt photocathodes with varied Pt loadings for the (**B**) planar, (**C**) μ–pyramid, and (**D**) μ–cone morphologies.

This behavior indicated that either increased reflection into the internal volume of the array, or reduced parasitic absorption due to increased continuity of the film, reduced the optical losses in the catalyst layer. The values of $-V_{-10}$ for planar Si and μ-pyramidal Si

photocathodes, 87 mV and 80 mV respectively, were slightly higher than those observed for Si μ-cone arrays with at least 8 nm of Pt, despite complete coverage of the Si surface with 4 nm of Pt. Further increases to the thickness of the Pt, to 8 nm on planar Si, and to 16 nm on μ-pyramidal arrays, led to improved *ff* but resulted in $-J_{ph} < 10$ mA cm^{-2}. Despite the Pt catalyst covering just ~2% of the total surface area of the Si μ–cone array photocathode, the μ-cone geometry maintained a relatively low overpotential while simultaneously exhibiting a value of $-J_{ph}$ that was higher than the values exhibited by bare planar or random μ-pyramidal textured Si photocathodes.

The ideal regenerative cell efficiency (η_{IRC}) represents the efficiency of a photoelectrode operating in conjunction with a nonpolarizable counter electrode performing the reverse reaction of interest, and was used as a metric to compare the performance of various different photocathodes.[115] The η_{IRC} for n^+p-Si/Pt μ–cone photocathodes with 8 nm of Pt was 5.8 ± 1.1 %, with a best-performing device yielding η_{IRC} = 6.9%. The η_{IRC} for n^+p-Si/Pt μ–cone photocathodes with 16 nm Pt and 4 nm of titanium was 6.7 ± 2.4 %, with a best-performing device yielding η_{IRC} = 9.8%. The use of an n^+p-Si homojunction with 8 nm, 16 nm of Pt, or a Ti/Pt stack on Si μ-cones resulted in an open-circuit potential (E_{oc}) of 416 ± 15 mV, 402 ± 22 mV, and 416 ± 60 mV respectively, vs RHE, and yielded light-limited photocurrent densities at potentials > 0 V vs RHE. The E_{oc} values for the best-performing device were 431 mV for 8 nm Pt films and were 442 mV for 16 nm Pt films. Thus the open-circuit voltage was insensitive to the thickness of the catalyst layer but greater $|J_{ph}|$ was obtained with the inclusion of a Ti adhesion layer separating the Si/Pt interface. The primary difference between the

performance of best-performing devices and average devices thus arose from the higher photovoltages of best-performing devices relative to average photocathodes.

The planar and μ-pyramid Si photocathodes showed higher photovoltages than the μ–cone photocathodes (**Figure 4.2**), even though all of the photocathodes were diffusion doped by a nominally identical process (**A.4**). SEM images indicated that the Si μ–cone arrays had an ~12.5-fold increase in junction area compared to a planar Si electrode, leading to an expected decrease in E_{oc} of ~65 mV assuming a diode quality factor of 1.0.[116-117] Diffusion-doped, etched Si μ-wire based photocathodes for HER have been reported to exhibit E_{oc} up to 480 mV.[104] The observed E_{oc} of 440 mV for the highest-efficiency photocathodes thus suggests that more voltage was being lost than expected from the increase in surface area. The three-dimensional diffusion of P atoms is likely to preferentially dope the tips of the microcones, which could further enhance the recombination and thus lower the photovoltage.[118] Hence, optimization of the doping process at the tips of the microcones could potentially improve the photovoltage of similar devices.

When Pt was deposited to a thickness >4 nm, n^+p-Si/Pt photocathodes were stable under air exposure for a few days between fabrication and testing. These electrodes also reversibly passed anodic current, indicating that the Pt layer protected the Si from forming an insulating interfacial oxide layer. Even though the catalytic overpotential was not changed by increasing the thickness of Pt beyond 4 nm for n^+p-Si/Pt photocathodes with planar or μ-pyramid geometries, the increased thickness of the Pt layer thus beneficially improved the stability of these electrodes. The increased Pt thickness needed for stability decreased the amount of light transmitted into the Si and limited the photocurrent densities

obtainable from n^+p-Si/Pt planar and μ-pyramid photocathodes. In contrast, little or no loss of J_{ph} or *ff* accompanied the increase in Pt thickness (16 nm) required for stable performance of the n^+p-Si/Pt μ-cone array photocathodes. Extended testing of n^+p-Si/Pt μ-cone array photocathodes was performed using chronopotentiometry at -10 mA cm^{-2}. The potential of the photocathode drifted negative with time while E_{oc} remained relatively constant, indicating an increase in V_{-10} at the catalyst. The losses in photocurrent onset could be reversed by cleaning the photoelectrode in concentrated HCl/HNO_3 followed by deionized H_2O (**A.4**).

4.3.2 Si photocathodes with electrodeposited Co-P catalyst

Co-P, an earth abundant, active HER electrocatalyst, was used to explore the compatibility of Si μ-cone arrays with catalysts other than noble metals such as Pt. Additionally, on p-type Si, Co-P produces a photovoltage in the absence of a homojunction,[42] providing the opportunity to compare the behavior of systems that have an emitter, in n^+-p structures, with photocathodes that instead primarily rely on minority-carrier collection in the light absorber to determine the spatial location of interfacial photocurrent collection at the solid/catalyst/liquid interface. To fabricate such photocathodes, Co/Co-P was electrodeposited onto Si μ-cones using a narrow-band light-emitting diode with an intensity-averaged wavelength of 625 nm, until a charge density of 400 mC cm^{-2} was passed. The bare p-Si μ-cone arrays predominantly absorbed light at 625 nm at the tips of the μ-cones.[43] Due to deposition at mass-transport-limited current densities, photoelectrodeposition of the Co/Co-P film occurred preferentially at the tips of the Si μ-cones, producing clumps > 1 μm in diameter that shadowed the underlying array (**Figure 4.3A**). To obtain an active Co-P catalyst, excess Co was removed by extended

potential cycling in contact with 0.50 M H_2SO_4(aq) while under 100 mW cm^{-2} of simulated AM1.5 solar illumination.[42] Potential cycling resulted in a restructuring of the catalyst film into nanoscale islands that were located predominantly at the tips of the μ–cones (Figure 3b).

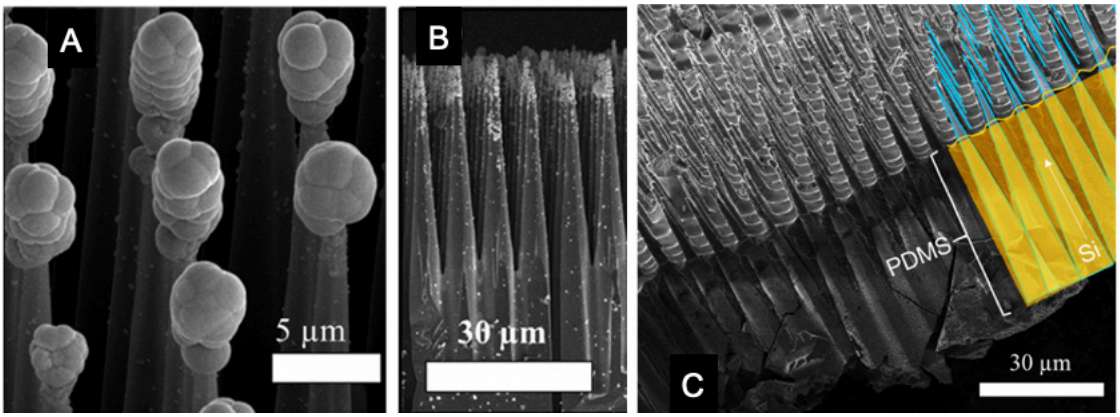

Figure 4.3: (**A**) Scanning-electron micrograph (SEM) of as-deposited Co/Co-P photoelectrodeposited onto the tips of p-Si μ-cones. The Co/Co-P loading, as determined by the charge density passed during the photoelectrodeposition, was 400 mC cm^{-2}. (**B**) SEM image of a cross section of a p-Si/Co-P μ–cone array after removal of excess Co by potential cycling in 0.50 M H_2SO_4(aq). (**C**) SEM of polymer embedded Si μ-cones removed from substrate, after deposition of Co-P and potential cycling in 0.50 M H_2SO_4(aq).

Figure 4.4 shows the *J-E* behavior of an illuminated bare p-Si μ–cone array photocathode, as well as the evolution of the *J-E* behavior of a p-Si/Co-P μ–cone array photocathode operated in contact with 0.50 M H_2SO_4(aq). Both J_{ph} and E_{oc} of the p-Si/Co-P μ–cone array photocathode improved with cycling and began to stabilize after ~ 16 voltammetric *J-E* cycles. Deposition of Co-P on planar, μ-pyramid, or μ-wire Si photocathodes yielded $-J_{ph}$ of 15 mA cm^{-2}, 20 mA cm^{-2}, and 25 mA cm^{-2} respectively [42], whereas p-type Si μ-cone/Co-P photocathodes exhibited $-J_{ph} = 32 \pm 2$ mA cm^{-2}. Compared

to bare p-type Si μ-cone array photocathodes, the deposition of Co-P on the Si μ-cone tips resulted in an average decrease in $-J_{ph}$ of 3 mA cm^{-2}. Si μ-cone array photocathodes exhibited $-J_{RHE}$ = 29 ± 2 mA cm^{-2} compared to $-J_{RHE}$ = 13 mA cm^{-2}, 18 mA cm^{-2}, and 22 mA cm^{-2} from planar, μ-pyramidal, and μ-wire array Si photocathodes, respectively,[42] demonstrating the beneficial light trapping properties of the Si μ-cone morphology when coupled with the Co-P HER catalyst.

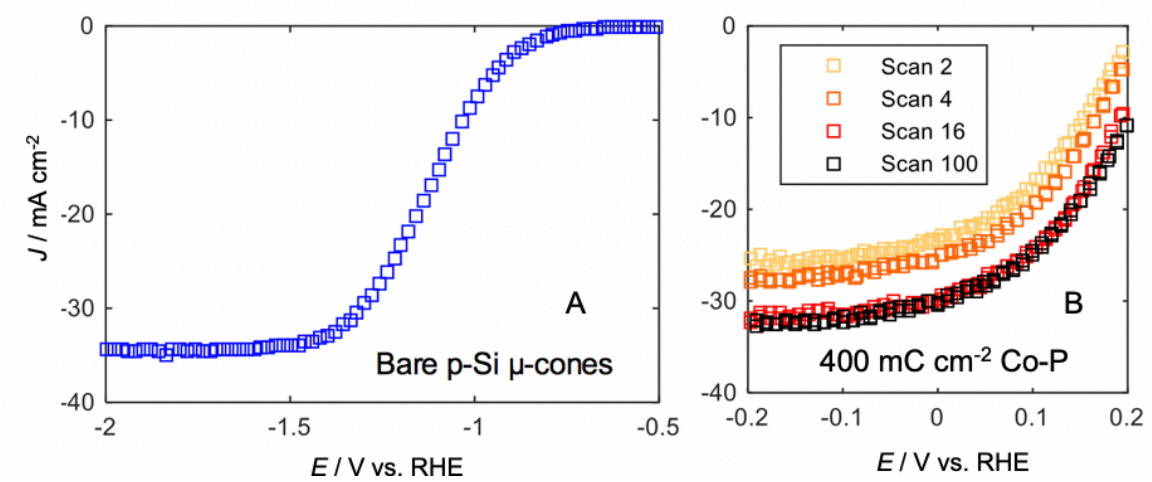

Figure 4.4: *J-E* behavior of p-Si μ-cone array photocathodes immersed in H_2-saturated 0.50 M H_2SO_4(aq), illuminated with 100 mW cm^{-2} of simulated AM1.5 illumination, and with rapid stirring. *J-E* behavior (**A**) prior to catalyst deposition and (**B**) after being loaded with Co/CoP after 2, 4, 16, and 100 scans from -0.376 V to +0.224 V vs RHE at 50 mV s^{-1}. The first and last scans were recorded after 20 s and 40 min, respectively.

The average E_{oc} for the p-Si/Co-P μ-cone array photocathodes was 331 ± 50 mV vs RHE, and the highest observed E_{oc} for the p-Si/Co-P μ-cone photocathodes was 384 mV vs RHE. The p-Si/Co-P μ-cone array photocathodes did not require a diffusion-doped homojunction but yielded lower E_{oc} values than the n$^+$p-Si/Pt μ-cone array photoelectrodes. The p-Si/Co-P μ-cone array photocathodes reached a solar-to-fuel current density of -10 mA cm^{-2} at +197 ± 20 mV vs RHE. The best-performing device exhibited this current

density at +220 mV versus RHE, with η_{IRC} = 3.1%. Extended testing of p-Si/Co-P μ-cone array photocathodes at 0 V vs RHE showed that after the initial increase in $|J_{ph}|$ during the first 30 min of cycling, the optical properties of the device remained stable for 24 h (**Figure 4.5**). SEM images of electrodes before and after extended testing in 0.50 M H_2SO_4(aq) showed that the structure of the Si μ-cone array was unchanged whereas the Co-P catalyst layer had restructured from μm-scale particles to nanoscale islands (**Figure 4.5**).

Figure 4.6A compares the reflectance in the wavelength range of 400 nm – 1100 nm for bare Si μ-cone array, a Si μ-cone array with 8 nm or 16 nm of Pt selectively deposited at the tips of the μ-cones, and a p-Si/Co-P μ-cone array electrode. No substantial change was observed in reflectance between n^+p-Si μ-cone arrays with and without a Pt coating, indicating that the incident light that is typically reflected from planar or μ-pyramid Si surfaces was redirected into the Si substrate due to the conical geometry. Hence, the Si μ-cone arrays had superior light-trapping properties relative to the bare Si pyramid structures before and after deposition of the catalyst. This concept is similar to that observed previously in effectively transparent contacts for silicon solar cells.[45, 119-120]

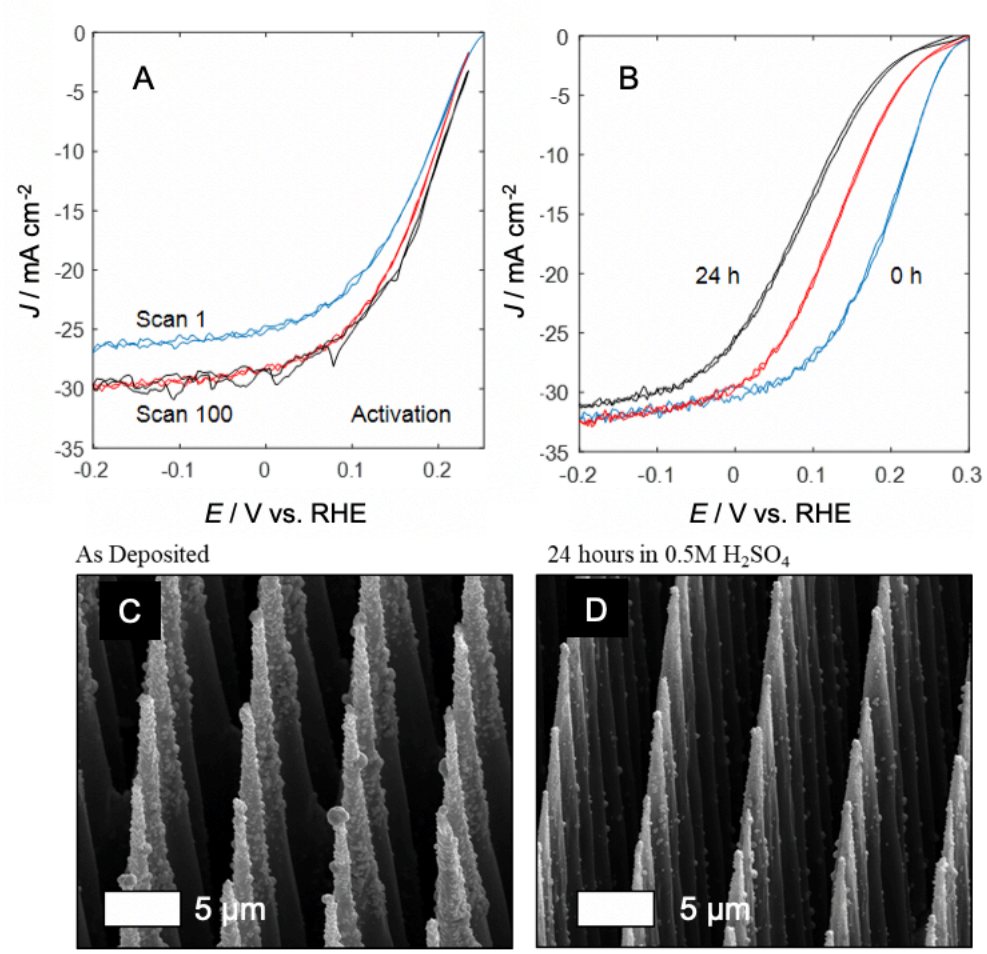

Figure 4.5: Extended photoelectrochemical testing of a p-Si/CoP µ-cone photocathode with 400 mC cm^{-2} Co-P. (**A**) Current density vs potential behavior in H_2-saturated 0.50 M H_2SO_4(aq) under 100 mW cm^{-2} of simulated AM1.5 illumination, with rapid stirring of the electrolyte for the 1st, 10th, and 100th cycle at 50 mV s^{-1}, blue, red, and black circles, respectively. The 100th scan occurred after 30 min of cycling. (**B**) Comparison of the *J-E* behavior over 24 h of continuous H_2(g) evolution at RHE under 1-Sun illumination for the device activated in (A). **(C-D)** Scanning-electron micrographs of the p-Si/CoP µ-cone photocathode with 400 mC cm^{-2} Co-P before (C) and after (D) testing in 0.50 M H_2SO_4(aq) under 1-Sun illumination for 24 h. Scale bars represent 5 µm at 0 degrees tilt.

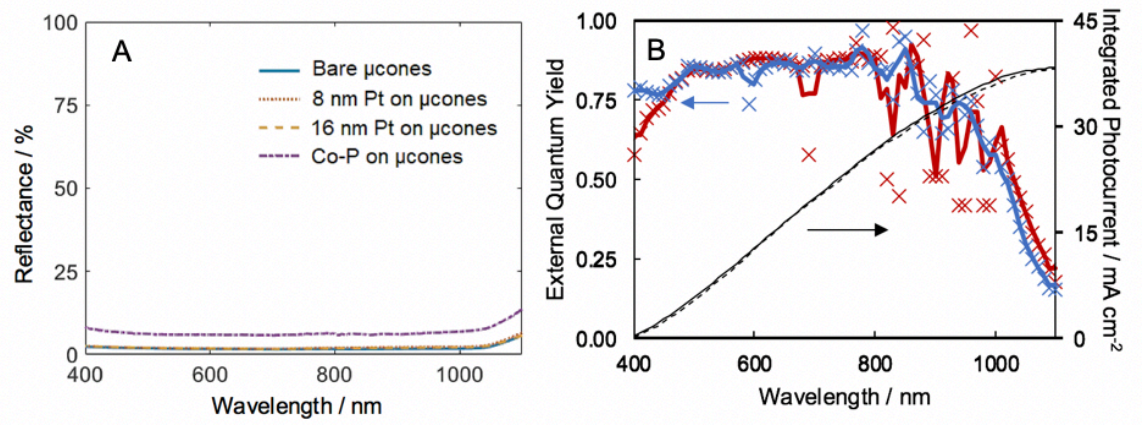

Figure 4.6: (**A**) Reflectance measurement of bare Si μ-cone arrays, Si μ-cone arrays with 8 and 16 nm of Pt or Co-P on their tips, as measured using a Cary 5000 UV-Vis-NIR with an integrating sphere. (**B**) Spectral response of a n^+p-Si/Pt μ-cone array at 0 V RHE (red) and p-Si μ-cone array in with 400 mC cm^{-2} Co-P at -200 mV vs RHE after activation in H_2 saturated 0.50 M H_2SO_4 for 30 min (blue). Individual data points were recorded every 10 nm, with a continuous line plotting the midpoint average for three data points. The maximum integrated photocurrent is plotted as a black line for a p-Si/Co-P μ-cone array (continuous) and n^+p-Si/Pt μ-cone array (dashed) from 400 nm to 1100 nm based on the photon density of the AM1.5 spectrum.

The reflectance of the p-Si/Co-P μ-cone array was 5% higher than the reflectance of the n^+p-Si/Pt μ-cone array because the Co-P islands were rough compared to the sputtered Pt coating, allowing relatively higher outward scattering of light from the Co-P islands on the tips of the μ-cones. Although the p-Si/Co-P μ-cones exhibited higher reflectance than the Pt-loaded μ-cones, the average J_{ph} was the same (-32 mA cm^{-2}) for p-Si/Co-P μ-cone arrays and n^+p-Si/Pt μ-cone arrays with 16 nm of Pt, indicating that in the 400 nm – 1100 nm wavelength range, 16 nm of Pt has a higher parasitic absorption than Co-P. Figure 5b compares the spectral response of an n^+p-Si/Ti/Pt μ-cone array to a p-Si/Co-P μ-cone array in 0.50 M H_2SO_4(aq) at 0 V and -0.2 V vs RHE, respectively. Both

photocathodes exhibited external quantum yields, defined as the fraction of photons collected as photocurrent, $\phi_{ext}(\lambda)$, in excess of 0.8 for wavelengths between 450-900 nm. The integrated photocurrent density for the AM1.5 spectrum was calculated via **Equation 4.1**:

$$J_{ph} = \frac{q}{hc}\int_{400\text{ nm}}^{1100\text{ nm}} \phi_{ext}(\lambda)\cdot P_{AM1.5}(\lambda)\cdot d\lambda \qquad (4.1)$$

where $P_{AM1.5}(\lambda)$ is the power density per cm^2 of the AM1.5 spectrum at the specified wavelength. The predicted limiting photocurrent density under AM1.5 illumination was in excellent accord with the measured J_{ph}.

Bare p-type Si μ-cone arrays were also embedded in polydimethylsiloxane (PDMS), peeled off the substrate, and fabricated into electrodes by deposition of a Au back contact using electron-beam evaporation (see Methods for more detail). **Figure 4.3C** shows a SEM image of Si μ-cone arrays in PDMS with ~ 15 μm of the tips exposed, with the freestanding, polymer-embedded μ-cones arrays decorated with Co-P using the same procedure as described for the on-substrate p-type Si μ-cones. Free-standing devices were tested as photocathodes in 0.50 M H_2SO_4(aq), to evaluate the performance of μ-cones in a membrane-embedded photocathode for H_2(g) generation. **Figure 4.7** presents representative *J-E* data in 0.50 M H_2SO_4(aq) under 100 mW cm^{-2} of simulated AM1.5 illumination. These devices exhibited E_{oc} = 150 ± 36 mV and J_{RHE} = -0.94 ± 0.32 mA cm^{-2}, with a best-performing device exhibiting J_{RHE} = -1.41 mA cm^{-2}. At -200 mV vs RHE, free-standing Si μ-cones exhibited an average J_{ph} = -6.5 mA cm^{-2}, and the best-performing device exhibited J_{ph} = -8.1 mA cm^{-2} and remained active for 3 h of testing.

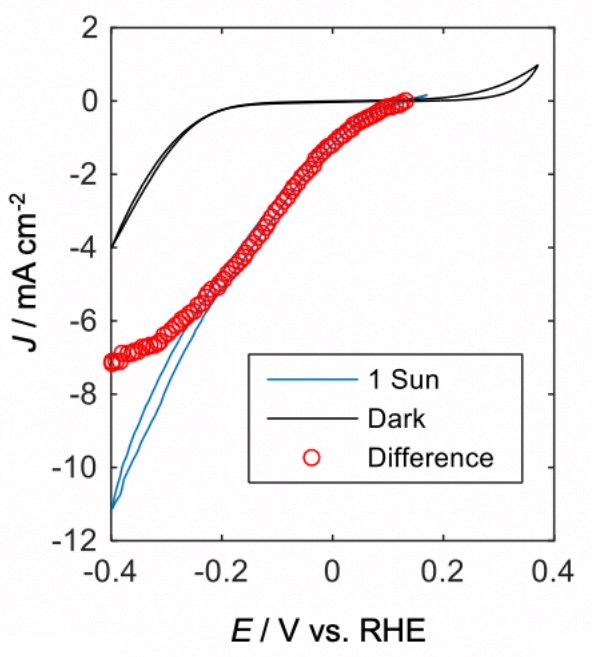

Figure 4.7: Representative *J-E* behavior of PDMS-embedded Si μ–cone array photocathodes decorated with Co-P and tested in 0.50 M H_2SO_4(aq) under 100 mW cm^{-2} of simulated AM1.5 illumination (blue). For comparison, the *J-E* behavior was recorded in the absence of illumination (black), and the difference between the two measured values was taken to be the photocurrent density for a given potential (red circle)

The photoactivity indicated that many of the individual p-type Si μ-cones were directly contacted with electrolyte during the Co-P catalyst deposition, and also while being tested as photocathodes. The absolute photocurrent density was higher than previous reports for Si μ-wires embedded in polymer membranes,[31, 39, 121] but lower than the photocurrent density for Si μ-cones on a substrate. Incomplete contact between the Au back contact and individual Si μ-cones may be responsible for the reduced photon collection of the free-standing array fabricated for proof-of-concept purposes in this work. Further optimization of the placement of the catalysts, in order to more optimally match local carrier generation rate, could be achieved using light-guided deposition of catalysts.[122]

The p-Si μ-cone/Co-P photocathodes do not require formation of a homojunction or emitter layer. Use of surface passivation and/or a homojunction or amorphous silicon heterojunction on the Si μ-cone arrays could thus improve the efficiency by reducing surface recombination velocities while retaining the benefit of high light absorption in Si μ-cones. Si μ-cones with < 100 cm s^{-1} surface passivation can in principle produce E_{oc} > 650 mV,[43, 101] and membrane-embedded μ-cones absorb > 90% of the light relative to their on-substrate counterpart. Polymer-embedded Si μ-cone arrays could thus produce $-J_{ph}$ > 25 mA cm^{-2}. Under standard conditions, HI splitting requires a minimum voltage of ~ 0.53 V, so utilizing a highly active catalyst such as Pt for the HER, along with improving the current collection could lead to flexible membrane-embedded photocathodes for HI splitting potentially reaching η_{IRC} > 10%.

Microcone array photoelectrodes can principle be fabricated in a scalable manner over large areas either by controlled electrochemical etching and/or by transferring the microcone arrays into peeled polymer films with subsequent re-use of the patterned growth substrate (**Scheme 4.1**) .[123] The approach of structuring a photoelectrode, in which both the absorber and electrocatalyst are in the illumination path, into microcone arrays provides a general strategy for optimization of light absorption in the photoelectrode without producing obscuration by high mass loadings of optically absorbing and/or reflecting electrocatalyst films often required for the low-overpotential production of fuel and/or for efficient water oxidation to O_2(g). Photoelectrodes utilizing Si μ-cones could additionally be implemented as a tandem junction to produce photovoltages necessary for water-splitting, with a wider band gap material deposited on the surface of the cones, in a similar fashion to previous studies that used a core-shell design on Si microwire arrays (**Scheme**

4.1).[124-125] In a core-shell tandem device, both semiconductors and one of two electrocatalysts would be on the sunlight-facing side of the membrane. Mesoscale metal films avoid parasitic absorption of photons due to resonant coupling,[120] thus Si μ-cone arrays are an advantageous scaffold for integrating wide band gap semiconductors in an architecture which can minimize reflection by the electrocatalyst in the illumination path.

Designs that utilize planar photoelectrodes integrated in a monolithic stack have consistently demonstrated the highest efficiencies for unassisted water splitting.[21, 48, 126] In microstructured electrodes, losses due to the increased area available for recombination at the charge-separating junction lead to lower photovoltages in comparison to planar devices.[103] GaAs microcells that have been transfer printed following epitaxial growth onto devices that used separate surfaces for light absorption and catalysis exhibited high efficiencies when normalized to the active area of the photovoltaics.[127] Printed assemblies of high-efficiency photovoltaics, wired to catalysts that are outside the optical path of incident light, thus could be integrated with ion-exchange membranes to ensure long term, stable sunlight-driven water splitting. However, such devices will necessarily encounter losses in active area when integrating the electrocatalysts and ion conducting membranes necessary for efficient and safe operation, limiting the maximum achievable photocurrent density from such systems. The increased theoretical photocurrent density that could be obtained by appropriately integrated mesoscale-structured semiconductors, electrocatalysts, and ion-exchange membranes may be able offset the losses in photovoltage associated with structured semiconductors, motivating further study into such systems.

4.4 Conclusion

High photocurrent densities were exhibited by n^+p-Si/Pt and p-Si/Co-P μ-cone array photocathodes when either Pt or Co-P hydrogen-evolution catalysts were deposited on the tips of the μ–cones. N^+p-Si/Pt μ–cone array photocathodes yielded an average η_{IRC} of 5.7% at the maximum power point, and best-performing n^+p-Si/Ti/Pt μ–cone devices yielded η_{IRC} = 9.8%. Thick (~16 nm) Pt and Co-P deposited onto Si μ-cone arrays produced only a 6% reduction in photocurrent density compared to bare photocathodes having the same morphology and microstructure. However, the Si μ–cone arrays exhibited photovoltages that were lower in magnitude by > 100 mV than the photovoltages obtained on planar or μ-pyramidally textured Si photocathodes. The photovoltage of the Si μ-cone arrays may be improved by optimizing the homojunction doping distribution. Greater than 90% of the incident light is absorbed in the μ–cones, as opposed to by the p-Si substrate at the base of the μ–cones,[43, 101] so removal of the μ–cones from the substrate will result in confinement of light in an effectively thin silicon absorber layer, facilitating that higher photovoltages from the μ–cone arrays provided that surface recombination can be minimized.[119] The p-Si/Co-P devices showed an average open-circuit voltage of 331 mV vs RHE without an emitter, which in combination with J_{ph} = -32 mA cm^{-2} resulted in η_{IRC} = 3.1%. Substantial improvements to the photovoltage obtained at the Si/Co-P junction will be required for such μ–cone arrays to be used as a practical photocathode in a tandem device. As a proof of concept, Si μ-cone arrays were also embedded in a flexible polymeric membrane, allowing for high catalyst loadings with minimal losses in photocurrent due to catalyst obscuration, and operation in a form factor which could facilitate integration into a tandem device for unassisted sunlight-driven water splitting.